Advanced Journal of Chemistry, Section A

Journal homepage: www.ajchem-a.com

Original Research Article

GC-MS Phytochemical Profiling and Computational Analysis of *Butea monosperma* Plant for Antidiabetic *α*-Amylase Inhibition

Rupasrre Peruru[1], Manasa Sathoori[2], Venkata Ramana Singamaneni[3]*, Pradeep Vidiyala[4], Ramenani Hari Babu[5], Om M. Bagade[6], Reehana Shaik[7], CH. K. V. L. S. N Anjana Male[8]*

[1] *Department of Pharmacology, Apollo Institute of Pharmaceutical Sciences, The Apollo University, Chittoor, Andhra Pradesh, India*
[2]*Joginpally B R Pharmacy College, Yenkapally, Moinabad, Ranga Reddy 500075, Telangana, India*
[3]*Department of Analytical Research and Development Cambrex, Charles City, Iowa- 50616, United State*
[4]*Department of Analytical Chemistry, Elixir Medical Corporation 920 N McCarthy Blvd 100, Milpitas, CA 95035, United State*
[5]*Department of Pharmacy Practice. Teerthanker Mahaveer College of Pharmacy, Teerthanker Mahaveer University, Moradabad 244001, Uttar Pradesh, India*
[6]*School of Pharmacy, Vishwakarma University, Pune-48, Maharashtra, India*
[7]*Department of Pharmaceutical Analysis, KL College of Pharmacy, KL University, KLEF, Vaddeswaram, Guntur-522502, India*
[8]*Indian Collaborations, School of Pharmacy, ITM University, Gwalior Madhya Pradesh, India*

ARTICLEINFO

Article history

Submitted: 2026-01-09
Revised: 2026-02-10
Accepted: 2026-02-15
ID: AJCA-2601-2024
DOI: 10.48309/AJCA.2026.571603.2024

KEYWORDS

Butea monosperma
GC–MS analysis
α-Amylase inhibition
In silico computational analysis
Phytochemical profiling
Antidiabetic potential

ABSTRACT

Butea monosperma is a traditional medicinal plant with antidiabetic and anti-inflammatory properties. This study aimed to investigate its *α*-amylase inhibitory potential through physicochemical evaluation, GC–MS profiling, molecular docking, and ADMET analysis. The hydroalcoholic extract yielded 10.5 % recovery. Physicochemical assessments confirmed acceptable ash values, low moisture content, and absence of heavy metals, pesticides, and pathogenic organisms. Phytochemical screening revealed abundant phenolics and flavonoids along with moderate levels of tannins, saponins, and cardiac glycosides, indicating the presence of bioactive secondary metabolites. GC–MS analysis identified 55 compounds, predominantly cyclic dipeptides, phenolic acids, phenolic alcohols, aromatic acids, fatty acids, and minor sterols. The major constituents include L-prolyl-L-valine, 3,6-diisopropylpiperazin-2,5-dione, hydrocinnamic acid, tyrosol, and benzeneacetic acid, as compounds associated with antioxidant, antimicrobial, anti-inflammatory, and cardioprotective activities. Molecular docking against *α*-amylase (PDB ID: 6Z8L) demonstrated that several phytochemicals exhibited binding affinities comparable to or stronger than that of the native ligand (–4.2 kcal/mol). Cholesta-4,6-dien-3-ol (–6.4 kcal/mol), indole-3-methyl (–4.9 kcal/mol), and di-isononyl phthalate (–4.8 kcal/mol) formed stable interactions with key catalytic residues ASP206, TRP203, and LYS140. ADMET analysis highlighted the favorable druglikeness of small phenolic molecules, such as hydrocinnamic acid, apocynin, *t*-butylhydroquinone, tyrosol, and L-prolyl-L-valine, which showed improved safety and pharmacokinetic profiles relative to the native ligand. Collectively, these findings affirm *Butea monosperma* is a rich source of potential *α*-amylase inhibitors and support further *in vitro*, *in vivo*, and formulation-based investigations for antidiabetic therapeutic development.

* Corresponding author: Singamaneni, Venkata Ramana; Male, CH. K. V. L. S. N Anjana
✉ E-mail: ramana.singamaneni@outlook.com; anjanamale.sop@itmuniversity.ac.in

GRAPHICAL ABSTRACT

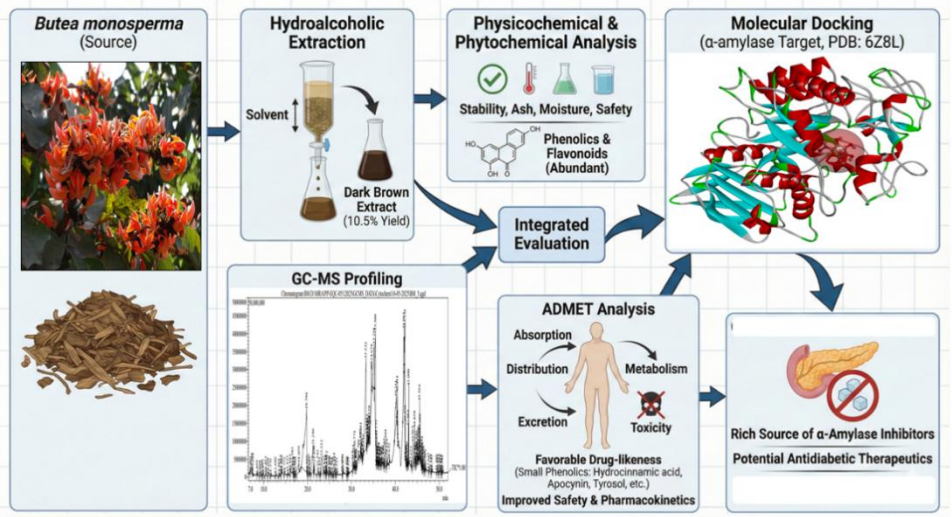

Introduction

Diabetes mellitus (DM) is a chronic metabolic disorder characterized by persistent hyperglycemia resulting from defects in insulin secretion, insulin action, or both. Type 2 diabetes mellitus (T2DM) is the most prevalent disease, affecting millions of people worldwide and contributing substantially to morbidity, mortality, and healthcare burden [1,2]. Postprandial hyperglycemia is a critical pathophysiological feature of T2DM and is strongly associated with complications, such as cardiovascular diseases, nephropathy, neuropathy, and retinopathy. One of the most effective strategies for attenuating postprandial glucose spikes is the inhibition of carbohydrate-hydrolyzing enzymes, particularly *α*-amylase, which catalyzes the breakdown of complex polysaccharides into glucose. Although synthetic *α*-amylase inhibitors, such as acarbose, voglibose, and miglitol, are commonly prescribed, their long-term use is associated with undesirable gastrointestinal side effects, including bloating, diarrhea, and abdominal discomfort. These limitations have shifted research interest toward plant-derived natural inhibitors that offer safer, more biocompatible, and sustainable alternatives [3–6]. Medicinal plants have long been recognized as powerful sources of bioactive metabolites with therapeutic potential. Among them, *Butea monosperma* (Lam.) Taub., belonging to the Fabaceae family, is an important traditional medicinal plant widely distributed across the tropical and subtropical regions of the Indian subcontinent [7–10]. It is popularly known as the "Flame of the Forest" due to its bright orange-red flowers and holds a prominent place in Ayurveda, Siddha, and Unani systems of medicine. Various parts of *Butea monosperma*, including the bark, leaves, flowers, and seeds, have traditionally been used to treat a wide range of disorders, such as inflammation, gastrointestinal illness, skin infections, parasitic diseases, and metabolic disturbances. Previous studies have reported the phytochemical composition of the plant, including flavonoids, phenolics, glycosides, terpenes, and alkaloids, which are well recognized for their antioxidant, anti-inflammatory, antimicrobial, and antidiabetic activities. These traditional claims, combined with emerging scientific interest, make B. monosperma a compelling candidate for detailed phytochemical and

computational studies targeting *α*-amylase inhibition [7–10].

Gas chromatography–mass spectrometry (GC–MS) is a powerful analytical tool widely used to characterize volatile and semi-volatile phytochemicals in complex plant extracts. This technique allows the precise identification of compounds based on retention time, mass fragmentation patterns, and spectral matching with established libraries. GC–MS profiling of medicinal plants has significantly advanced natural product research by enabling the discovery of novel bioactive compounds and supporting chemotaxonomic studies. In the context of antidiabetic research, GC–MS enables rapid screening of plant-derived metabolites that may contribute to enzyme inhibition, oxidative stress modulation, and metabolic regulation [11–13].

Computational methods such as molecular docking have emerged as essential tools in modern drug discovery. Docking provides structural insights into how phytoconstituents interact with target enzymes at the molecular level, enabling prediction of binding affinity, stability, and potential inhibitory mechanisms. Combined with *in silico* Absorption, Distribution, Metabolism, Excretion, and Toxicity (ADMET) analysis, this approach helps determine the pharmacokinetic behavior and safety profile of candidate molecules. Such integrated computational workflows significantly reduce experimental workload and accelerate the identification of promising lead compounds [14–17].

Given the increasing global prevalence of diabetes and the limitations of existing *α*-amylase inhibitors, there is growing demand for plant-based therapeutic alternatives that are effective, safe, and economically accessible. *Butea monosperma*, with its rich ethnomedicinal history and diverse phytochemical content, presents a promising opportunity for the discovery of natural enzyme inhibitors. However, comprehensive investigations combining phytochemical profiling and computational analyses targeting *α*-amylase inhibition remain limited.

Materials and Methods

Collection of plant material and extraction by percolation method

Butea monosperma plant material was collected in December 2024 from a local area of Nalgonda, Telangana, India. A herbarium specimen was prepared from the collected plant material and taxonomically authenticated by Dr. K. Madhava Chetty, Head, Department of Botany, Sri Venkateswara University, Tirupati–517502, Andhra Pradesh, India. Fresh leaves and bark were thoroughly cleaned with distilled water to remove adhering dust and debris, followed by shade drying at room temperature for seven days to preserve volatile phytoconstituents. The dried plant material (approximately 500 g) was coarsely powdered for further extraction. Extraction was performed using the percolation method with a hydroalcoholic solvent system comprising of ethanol and water (70:30). The powdered material was placed in a percolator, moistened with an adequate quantity of solvent, and allowed to macerate for 24 hours. Thereafter, continuous percolation was carried out by the addition of fresh solvent at regular intervals until complete exhaustion of the phytochemical constituents was confirmed by the appearance of a nearly colorless percolate. The pooled extracts were concentrated by natural evaporation in clean petri dishes and stored under appropriate conditions for subsequent phytochemical evaluation [18,19].

Physicochemical, phytochemical, and microbial evaluation

The extracts obtained through hydroalcoholic percolation were subjected to comprehensive

physicochemical and qualitative assessments using standard procedures. Organoleptic properties (color, odor, and taste) were evaluated visually and through sensory perception. The pH values of the 1 % and 10 % aqueous extract solutions were measured using a calibrated digital pH meter. Foreign matter was manually separated and calculated as a percentage of the total contamination. The moisture content was estimated through loss on drying at 105 °C until a constant weight was achieved. Ash values (total ash, acid-insoluble ash, sulfated ash, and water-soluble ash) were determined using controlled incineration and gravimetric analysis. The alcohol-soluble and water-soluble extractive values were measured by macerating the powdered drug in the respective solvents, filtering, drying, and calculating the percentage yields [20,21].

Heavy metal profiling was conducted using microwave digestion followed by atomic absorption spectrometry to quantify As, Cd, Pb, Hg, Zn, Cu, Cr, and Mn. Pesticide residue analysis involved concentrating the extract, purification through a clean-up column, and analysis by gas chromatography with an electron capture detector to ensure detection within the 0.1–0.5 ppb range [22,23].

Phytochemical screening of the percolated extract confirmed the presence of major secondary metabolites, including carbohydrates, proteins, lipids, glycosides, flavonoids, alkaloids, tannins, phenolics, saponins, and steroids using standard colorimetric and precipitation reactions. Microbial evaluation was performed through serial dilution and culture techniques to estimate total bacterial and fungal load, while specific pathogens, E. coli, Salmonella spp., Shigella spp., Pseudomonas aeruginosa, and Staphylococcus aureus, were identified using selective and differential media with confirmatory biochemical tests. All analyses were conducted under standardized laboratory conditions to ensure reliability and reproducibility [20,21,24–26].

GC–MS analysis

The hydroalcoholic extract of *Butea monosperma* was analyzed using GC–MS to characterize its volatile and semi-volatile constituents. The sample (BM) was injected at 1.0 µL using the programmed method PHYTOCHEM_1. qgm, and the chromatographic run was recorded in full-scan mode under standard operating conditions. The mass spectra generated across the complete retention window were automatically matched with the NIST 2020 mass spectral library for compound identification. All instrument parameters, including sample loading, scan settings, and tuning profiles, followed the validated phytochemical analysis protocol of the GC-MS system [27–30].

Molecular docking analysis

Molecular docking studies were performed to evaluate the interaction of *Butea monosperma* phytoconstituents with *α*-amylase (PDB ID: 6Z8L). Compounds identified by GC–MS analysis were selected as ligands for docking. The 2D structures were sketched using ChemDraw, and the corresponding 3D structures were retrieved or cross-verified from PubChem. All ligands were energy-minimized and converted to PDBQT format using Open Babel integrated within PyRx (AutoDock Vina) [15–17].

The crystal structure of *α*-amylase (6Z8L) was downloaded from the RCSB Protein Data Bank and prepared using Discovery Studio by removing water molecules, heteroatoms, and co-crystallized ligands, followed by addition of polar hydrogens and appropriate force-field parameters. The prepared receptor was then saved in the PDBQT format. Docking was carried out in PyRx, where the grid box was centered on the active site of the protein using the coordinates X = −13.501833, Y = −0.843500, and Z = −1.625333.

Default exhaustiveness values were applied to achieve a balance between the accuracy and computational cost. Each GC-MS-identified compound was docked individually, and the lowest binding energy (kcal/mol) was recorded. Protein–ligand interactions, including hydrogen bonds, hydrophobic contacts, and active-site residue involvement, were analyzed and visualized using Discovery Studio Visualizer. A 3D ribbon view of alpha-amylase is shown in Figure 1.

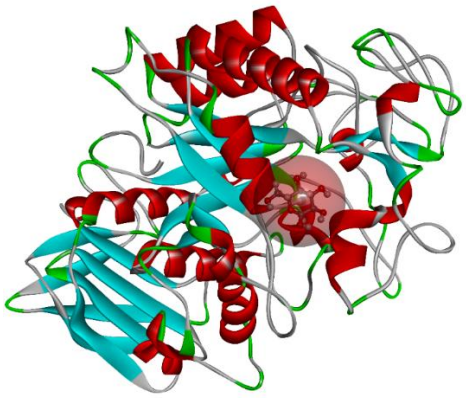

Figure 1. 3D ribbon view of alpha-amylase enzyme with active cavity

ADMET analysis

The ADMET properties of the GC–MS–identified phytoconstituents were evaluated using *in silico* prediction platforms, including SwissADME and ADMETlab 3.0. The ligand structures obtained from PubChem were optimized and converted using ChemDraw and Open Babel before submission to the prediction tools. Each compound was assessed for absorption parameters (Caco-2 permeability, P-gp interaction, Human Intestinal Absorption (HIA)), distribution (Plasma Protein Binding (PPB), Blood Brain Barrier (BBB) penetration), metabolism (CYP450 inhibition/substrate likelihood), excretion (clearance, half-life), and toxicity (Ames mutagenicity, hepatotoxicity, DILI, skin sensitization). All predicted values were compiled and compared with the native ligand (NL-6Z8L) to evaluate pharmacokinetic suitability and overall safety [31,32].

Results and Discussion

Organoleptic, physicochemical, microbial, and phytochemical evaluation

The hydroalcoholic extract of *Butea monosperma* yielded 10.5 % of a dark brown, slightly aromatic, bitter solid mass, characteristic of phenolic- and glycoside-rich plant materials. Physicochemical parameters indicated a near-neutral pH (6.8 for 1 % and 6.3 for 10 % solutions), acceptable ash values, and low moisture content, confirming good purity and stability (Table 1). A higher alcohol-soluble extractive value compared to the water-soluble content suggested the efficient extraction of semi-polar metabolites. Heavy metal and pesticide analyses did not reveal any detectable contaminants. Microbial evaluation confirmed the absence of pathogens, such as E. coli, Salmonella, Shigella, P. aeruginosa, and S. aureus, supporting the microbial safety of the extract.

Phytochemical screening of the hydroalcoholic extract of *Butea monosperma* demonstrated a strong abundance of phenolic compounds and flavonoids (+++), confirming the presence of potent antioxidant and anti-inflammatory constituents. Moderate levels of tannins, saponin glycosides, cardiac glycosides, and anthraquinone glycosides (++) suggest additional pharmacological roles, such as antimicrobial, cardiotonic, and wound-healing benefits. Trace amounts of alkaloids (+), proteins (+), and amino acids (+) were detected, indicating the presence of minor nitrogenous components that may contribute to nutritional or biochemical activity.

Table 1. Organoleptic, physicochemical, microbial, and phytochemical evaluation of the hydroalcoholic extract of *Butea monosperma*

Parameter category	Evaluated parameter	Observation / Result
Organoleptic properties	Colour	Dark brown
	Odour	Slightly aromatic
	Taste	Bitter
Physicochemical parameters	Extract Yield	10.5 % (w/w) solid mass
	pH (1 % solution)	6.8
	pH (10 % solution)	6.3
	Total Ash	7.81 %
	Acid-Insoluble Ash	1.22 %
	Water-Soluble Ash	2.97 %
	Sulphated Ash	1.32 %
	Loss on Drying (Moisture)	4.67 %
	Alcohol-Soluble Extractive	17.97 %
	Water-Soluble Extractive	14.56 %
	Heavy Metals	Not detected
	Pesticide Residues	Not detected
Microbial evaluation	*E. coli*	Absent
	Salmonella spp.	Absent
	Shigella spp.	Absent
	Pseudomonas aeruginosa	Absent
	Staphylococcus aureus	Absent
Phytochemical screening	Phenolic Compounds	+++ (Abundant)
	Flavonoids	+++ (Abundant)
	Tannins	++ (Moderate)
	Saponin Glycosides	++ (Moderate)
	Cardiac Glycosides	++ (Moderate)
	Anthraquinone Glycosides	++ (Moderate)
	Alkaloids	+ (Trace)
	Coumarins	Absent
	Quinones	Absent
	Triterpenoids	Absent
	Carbohydrates	Absent
	Proteins	+ (Trace)
	Amino Acids	+ (Trace)
	Fats & Oils	Absent
	Steroids	Absent

Conversely, carbohydrates, fats, oils, steroids, triterpenoids, coumarins, and quinones were absent, highlighting the efficiency of the solvent in selectively extracting secondary metabolites. Overall, the extract exhibited a phytochemical profile dominated by polyphenols, flavonoids, and glycosides, supporting its potential antioxidant, anti-inflammatory, antimicrobial, cardioprotective, and α-amylase-inhibitory applications.

GC-MS analysis

GC–MS analysis of the hydroalcoholic extract of *Butea monosperma* revealed a chemically diverse profile comprising 55 distinct chromatographic

peaks, reflecting the presence of multiple phytoconstituent classes (Table 2 and Figure 2). Several bioactive compounds were identified based on retention time, peak area contribution, and high NIST library match scores. The chromatographic pattern was dominated by cyclic dipeptides, phenolic acids, phenolic alcohols, aromatic acids, fatty acids, sterols, and minor lipid derivatives, indicating the presence of a broad spectrum of secondary metabolites.

The most prominent constituent was Cyclo(L-prolyl-L-valine) (retention time 33.35 min; 13.28 %), a diketopiperazine-type cyclic dipeptide known for strong antioxidant, antimicrobial, and anti-inflammatory activities and commonly associated with plant defense responses. Another abundant compound, 3,6-diisopropylpiperazin-2,5-dione (4.72 %), further supported the presence of bioactive peptide derivatives in the extract.

Table 2. Major GC–MS identified compounds in *butea monosperma* hydroalcoholic extract

Compound name	Retention time (min)	Area (%)	Phytochemical class	Pharmacological relevance
L-Prolyl-L-valine	33.35	13.28	Cyclic dipeptide	Antioxidant, antimicrobial, anti-inflammatory
3,6-Diisopropylpiperazin-2,5-dione	34.67	4.72	Cyclic dipeptide	Antioxidant, cytoprotective
Hydrocinnamic acid	20.27 / 21.29	3.84	Phenolic acid	Anti-inflammatory, antioxidant
Tyrosol	23.23	2.39	Phenolic alcohol	Neuroprotective, cardioprotective, antioxidant
Benzeneacetic acid	18.05	1.88	Aromatic acid	Antioxidant, flavor/fragrance precursor
Bis(2-ethylhexyl) phthalate	43.09	1.23	Phthalate (contaminant)	Laboratory plasticizer (non-phytochemical)
Di-isononyl phthalate	45.87–46.63	0.71	Phthalate (contaminant)	Likely solvent/plastic artifact
Indole, 3-methyl-	21.49	0.28	Indolic compound	Antimicrobial, growth regulatory
Benzoic acid, 4-ethoxy-, ethyl ester	26.38	0.04	Aromatic ester	Antioxidant, fragrance agent
Apocynin	24.17	0.04	Phenolic ketone	Anti-inflammatory, NADPH oxidase inhibitor
***t*-Butylhydroquinone**	28.97	0.03	Phenolic antioxidant	Strong antioxidant, stabilizer
Cholesta-4,6-dien-3-ol	49.81	0.05	Sterol derivative	Anti-inflammatory, membrane support
3-((12-Acetoxyoctadecanoyl) oxy) propane-1,2-diyl diacetate	50.43	0.04	Glyceride derivative	Lipidic/waxy phytoconstituent

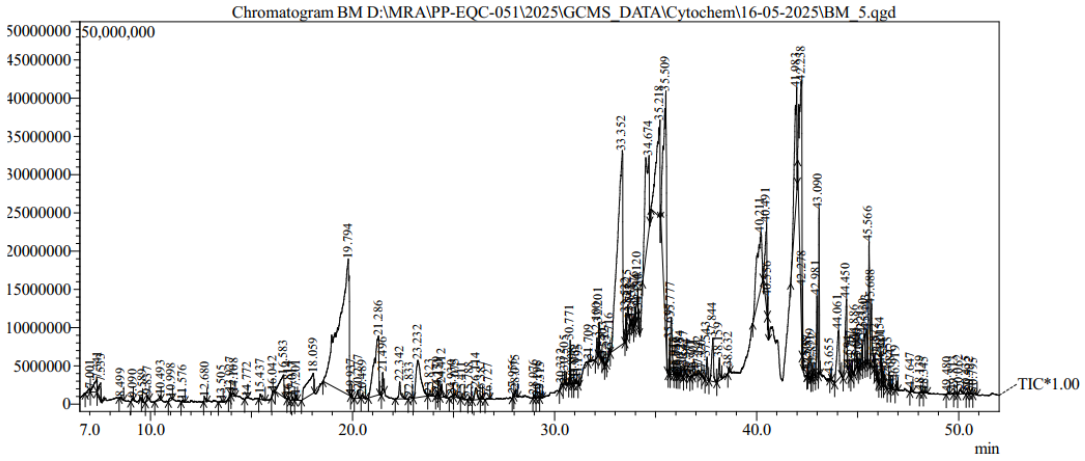

Figure 2. GC–MS chromatogram of the hydroalcoholic extract of *Butea monosperma*

Significant phenolic components, such as hydrocinnamic acid (3.84 %) and benzeneacetic acid (1.88 %), demonstrated the phenylpropanoid profile of the extract, contributing to its antioxidant, anti-inflammatory, and free radical-scavenging capacity. Similarly, tyrosol (2.39 %), a well-documented phenolic alcohol with neuroprotective and cardioprotective properties, further strengthened the antioxidant potential of the extract. Additional phenolic contributors, including apocynin, *t*-butylhydroquinone, and aromatic esters, such as benzoic acid, 4-ethoxy-, and ethyl ester, were detected in lower proportions, collectively reinforcing the plant's anti-inflammatory and redox-modulating properties.

The GC–MS profile also revealed the presence of fatty acids and lipid derivatives, such as oleic acid and complex glycerides, indicative of the lipidic and membrane-stabilizing components naturally occurring in plant tissues. Minor sterols, including cholesta-4,6-dien-3-ol, suggest the presence of phytosterol-related metabolites that are important for cell membrane regulation and potential anti-inflammatory effects. Trace detection of bis(2-ethylhexyl) phthalate and di-isononyl phthalate likely represents non-biological contaminants introduced through laboratory plasticware, as these are common analytical artifacts.

Overall, the GC–MS results demonstrated that *Butea monosperma* extract contains a rich profile of phenolic acids, phenolic alcohols, cyclic dipeptides, and fatty acids, many of which are well-established modulators of oxidative stress, inflammation, and microbial resistance. These findings align closely with the traditional medicinal uses of the plant and support its potential application in antioxidant, antimicrobial, anti-inflammatory, cardioprotective, and *α*-amylase inhibitory formulations.

Molecular docking analysis

The molecular docking study evaluated the alpha-amylase inhibitory potential of GC–MS–identified phytochemicals from *Butea monosperma* and compared their binding affinity and interaction profiles with the native ligand (NL-6Z8L) of PDB ID: 6Z8L (Table 3). The 2D and 3D docking interactions of all selected compounds and native ligands are shown in Table 4. The native ligand produced a docking score of –4.2 kcal/mol, forming strong conventional hydrogen bonds with ASP206 at multiple distances (1.93–3.06 Å) and hydrophobic π–π stacking interactions with TRP203, confirming its essential role in stabilizing the catalytic site.

Table 3. Binding interactions of selected compounds with alpha-amylase

Amino acid	Bond length	Bond type	Bond category	Ligand energy (Kcal/mol)	Docking score
NL-6Z8L					
ASP206	1.93104	Hydrogen Bond	Conventional Hydrogen Bond	447.08	-4.2
ASP206	2.46312				
LYS140	2.54804				
ASP206	3.06606				
TRP203	4.22272	Hydrophobic	Pi-Pi Stacked		
TRP203	3.92522				
3-((12-Acetoxyoctadecanoyl) oxy) propane-1,2-diyl_diacetate					
THR155	2.43215	Hydrogen Bond	Conventional Hydrogen Bond	1126.04	-4.2
ARG158	2.34001				
ARG158	2.43036				
ARG176	2.27874				
TRP203	3.99283	Hydrophobic	Pi-Sigma		
TRP203	5.12778		Pi-Alkyl		
3,6-Diisopropylpiperazin-2,5-dione					
ARG158	2.33436	Hydrogen Bond	Conventional Hydrogen Bond	260.78	-4.1
ARG158	2.23429				
TRP203	4.77111	Hydrophobic	Pi-Pi T-shaped		
PRO204	5.38312		Pi-Alkyl		
Apocynin					
LYS140	2.3855	Hydrogen Bond	Conventional Hydrogen Bond	56.13	-4.4
TRP203	4.30821	Hydrophobic	Pi-Pi Stacked		
TRP203	3.70921				
Benzeneacetic_acid					
ASP206	1.89112	Hydrogen Bond	Conventional Hydrogen Bond	78.26	-4.6
TRP203	4.23566	Hydrophobic	Pi-Pi Stacked		
TRP203	3.66939				
Benzoic acid, 4-ethoxy-, ethyl ester					
LYS140	2.31592	Hydrogen Bond	Conventional Hydrogen Bond	75.48	-4.5
ASP206	3.0079				
TRP203	4.09663	Hydrophobic	Pi-Pi Stacked		
TRP203	3.62524				
Bis(2-ethylhexyl) phthalate					
LYS140	2.35263	Hydrogen Bond	Conventional Hydrogen Bond	379.19	-4.1
TRP203	3.67107		Pi-Pi Stacked		
TRP203	4.31633	Hydrophobic			
PRO204	4.0872		Alkyl		
TRP203	4.95435		Pi-Alkyl		
Cholesta-4,6-dien-3-ol					

Amino acid	Bond length	Bond type	Bond category	Ligand energy (Kcal/mol)	Docking score
LYS140	2.39599	Hydrogen Bond	Conventional Hydrogen Bond	457.66	-6.4
TRP203	3.82228	Hydrophobic	Pi-Sigma		
PRO204	4.09121		Alkyl		
PRO204	4.21237				
TRP203	4.8758		Pi-Alkyl		
TRP203	4.3805				
TRP203	5.08908				
TRP203	5.18248				
TRP203	3.80178				
TRP203	5.1849				
TRP203	4.78595				
TRP203	4.91672				
TRP203	4.87263				
Di-isononyl_phthalate					
GLY205	3.01927	Hydrogen Bond	Conventional Hydrogen Bond	272.74	-4.8
ASP206	2.74255				
ASP206	3.6925		Carbon Hydrogen Bond		
TRP203	4.2065	Hydrophobic	Pi-Pi Stacked		
TRP203	3.6705				
ALA154	3.79125		Alkyl		
ILE242	4.28993				
ALA154	4.19715				
TRP203	5.12166		Pi-Alkyl		
Hydrocinnamic_acid					
ASP206	2.74737	Hydrogen Bond	Conventional Hydrogen Bond	67.34	-4.6
ARG176	2.59351				
TRP203	4.1866	Hydrophobic	Pi-Pi Stacked		
TRP203	3.63609				
Indole, 3-methyl-					
ASP206	2.19639	Hydrogen Bond	Conventional Hydrogen Bond	267.19	-4.9
TRP203	4.30172	Hydrophobic	Pi-Pi Stacked		
TRP203	4.88282				
TRP203	4.32201				
TRP203	3.66954				
TRP203	5.19933		Pi-Alkyl		
TRP203	4.65675				
L-prolyl-L-valine					
ASP206	2.6014	Hydrogen Bond	Conventional Hydrogen Bond	303.84	-4.4
ASP206	2.92004				
TRP203	3.12173	Hydrophobic	Pi-Donor Hydrogen Bond		
TRP203	3.98125		Pi-Sigma		

Amino acid	Bond length	Bond type	Bond category	Ligand energy (Kcal/mol)	Docking score
TRP203	3.69542	Hydrophobic			
			***t*-Butylhydroquinone**		
TRP203	4.28734	Hydrophobic	Pi-Pi Stacked	104.75	-4.6
TRP203	3.6464				
TRP203	4.84954		Pi-Alkyl		
TRP203	4.62547				
			Tyrosol		
TRP203	4.21016	Hydrophobic	Pi-Pi Stacked	167.16	-4.6
TRP203	3.6361				

Table 4. 3D and 2D docking interactions of all the selected compounds and NL-6Z8L

2D Docking interactions	3D Docking interactions
NL-6Z8L	
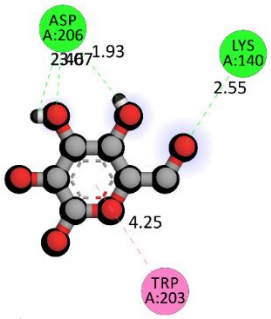	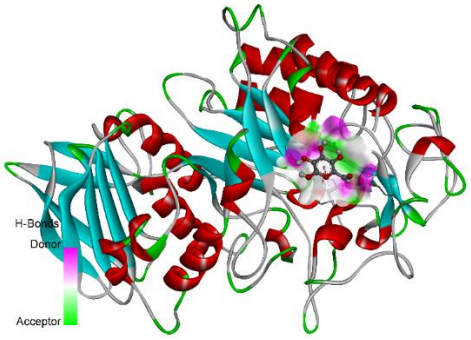
3-((12-Acetoxyoctadecanoyl) oxy) propane-1,2-diyl_diacetate	
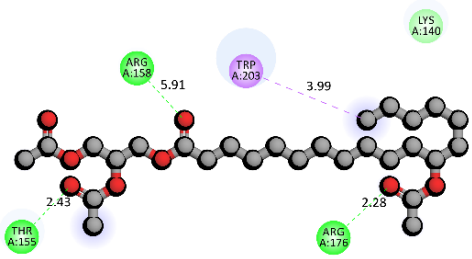	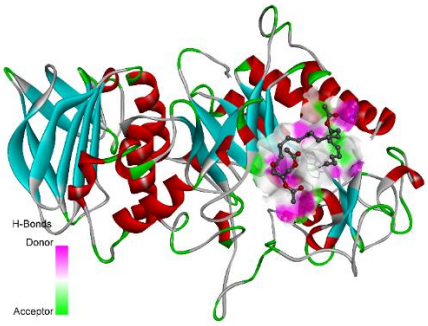
3,6-Diisopropylpiperazin-2,5-dione	
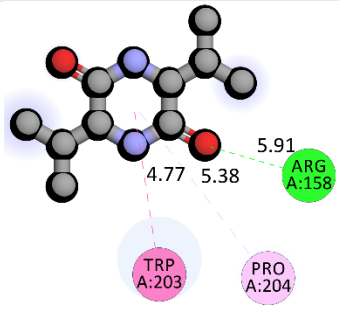	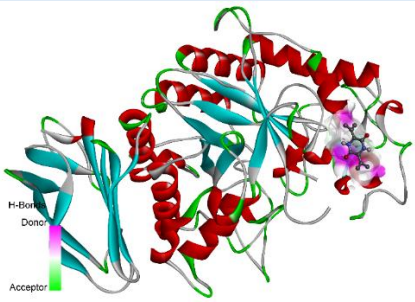

2D Docking interactions	3D Docking interactions
Apocynin	
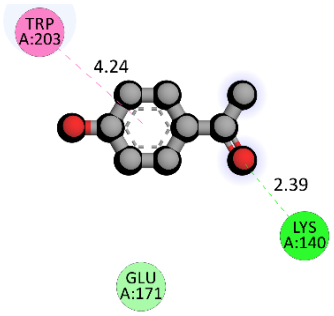	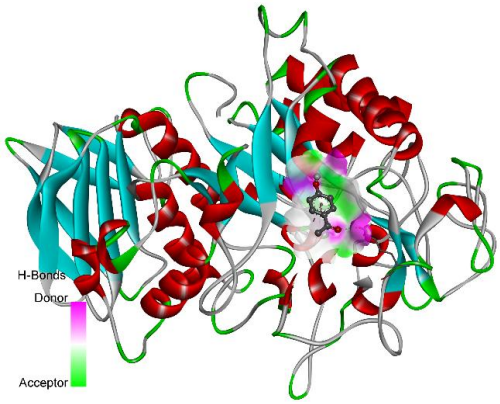
Benzeneacetic_acid	
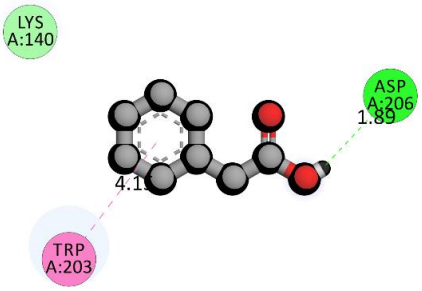	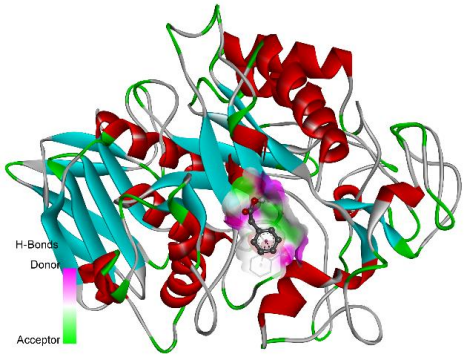
Benzoic_acid, _4-ethoxy-, _ethyl_ester	
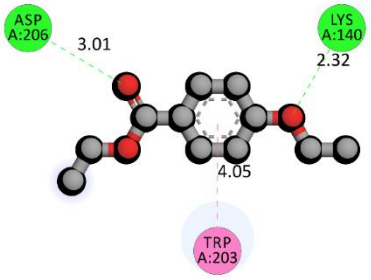	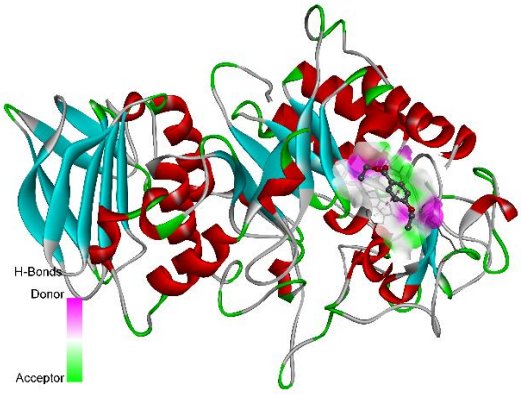
Bis(2-ethylhexyl) phthalate	
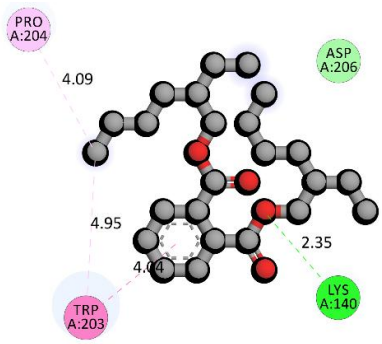	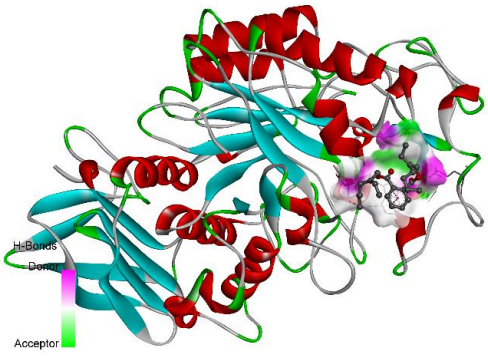

2D Docking interactions	3D Docking interactions
Cholesta-4,6-dien-3-ol	
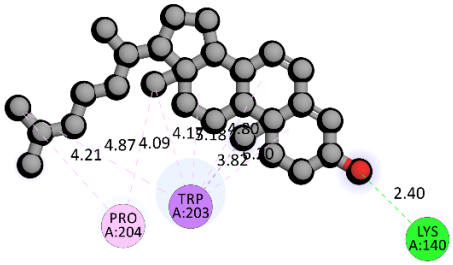	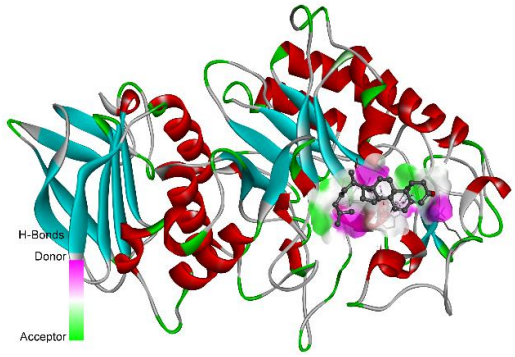
Di-isononyl_phthalate	
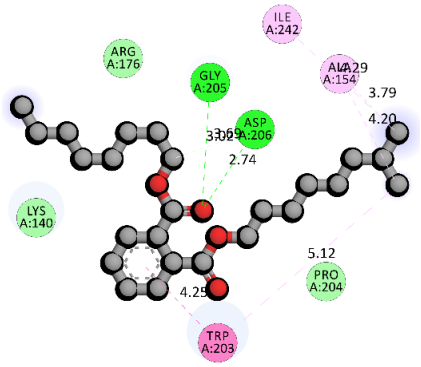	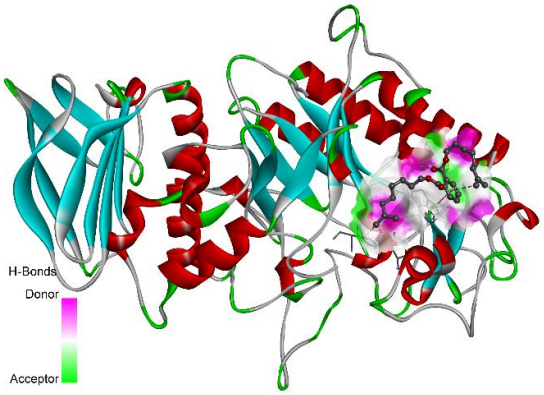
Hydrocinnamic_acid	
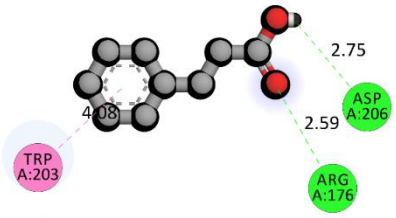	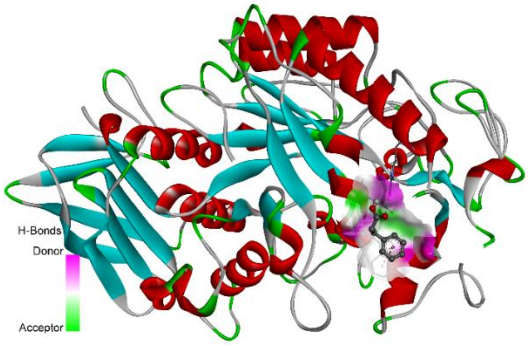
Indole, 3-methyl-	
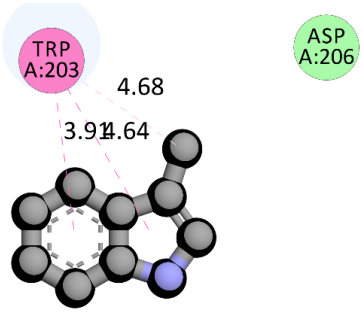	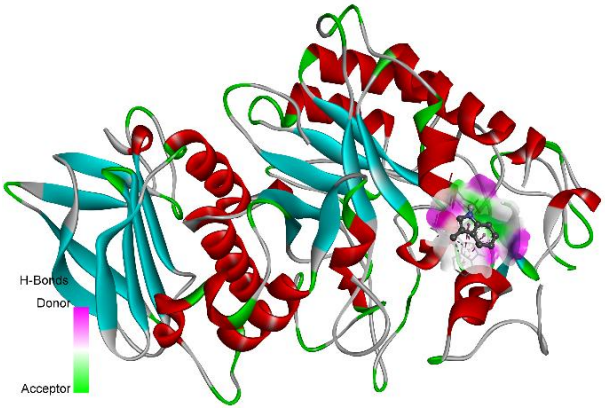

2D Docking interactions	3D Docking interactions
L-prolyl-L-valine	
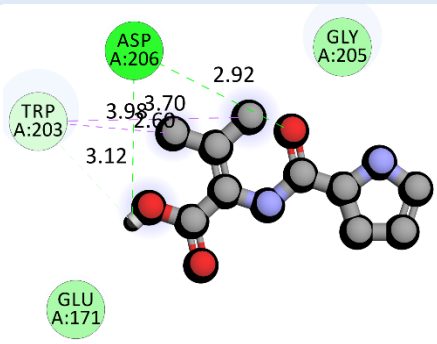	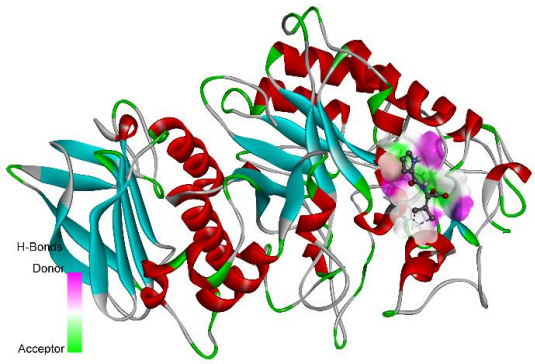
***t*-Butylhydroquinone**	
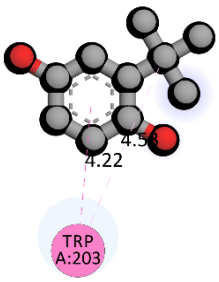	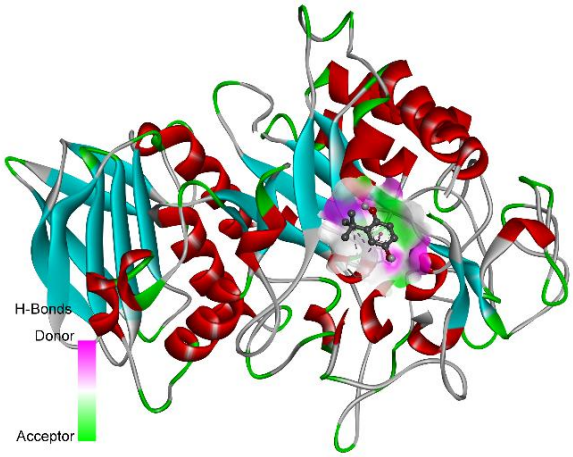
Tyrosol	
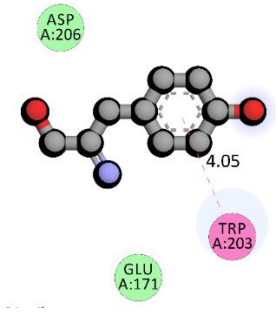	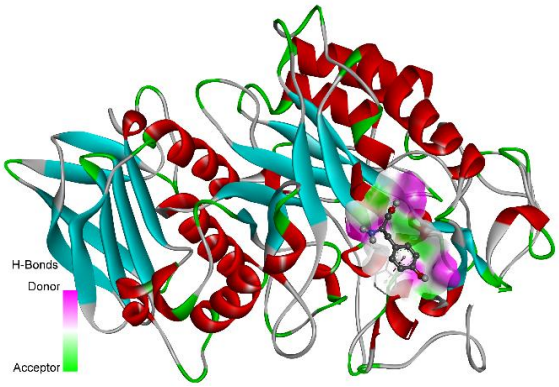

Thus, ASP206 and TRP203 served as key reference residues for evaluating ligand performance. Several phytochemicals have demonstrated equal or superior binding profiles relative to native ligands. Cholesta-4,6-dien-3-ol exhibited the strongest affinity (–6.4 kcal/mol), representing the most potent inhibitor candidate in this analysis. It retained critical hydrogen bonding with LYS140 while forming extensive hydrophobic contacts, especially multiple π-sigma and π-alkyl interactions, with TRP203 and PRO204, suggesting a highly stable fit within the hydrophobic pocket. Its broad interaction spectrum reflects favorable steric complementarity and enhanced binding stability compared to those of the native ligand.

Compounds such as Di-isononyl phthalate (–4.8 kcal/mol) and Indole, 3-methyl- (–4.9 kcal/mol) also surpassed the native ligand's docking score. Both formed hydrogen bonds with catalytic residues, particularly ASP206, similar to the native ligand, and strong π–π stacked interactions with TRP203, highlighting their ability to effectively interfere with substrate orientation and enzymatic catalysis. Moderate-affinity compounds including Benzeneacetic acid, Hydrocinnamic acid, *t*-Butylhydroquinone, and Tyrosol (–4.6 kcal/mol) consistently interacted with ASP206 and TRP203. Their preserved binding geometry indicates that smaller aromatic molecules can mimic the key interactions of the native ligand, particularly the π–π stacking essential for stabilizing the binding channel. Apocynin (–4.4 kcal/mol) and L-prolyl-L-valine (–4.4 kcal/mol) also engaged LYS140 or ASP206 through hydrogen bonding, suggesting enzyme–ligand compatibility, although with slightly lower stability. Meanwhile, bulky molecules like Bis(2-ethylhexyl) phthalate and cyclic dipeptides showed weaker docking scores (–4.1 kcal/mol), likely due to steric limitations affecting fit within the catalytic cleft.

Overall, the docking results indicated that several Butea monosperma constituents possess meaningful alpha-amylase inhibitory potential, with Cholesta-4,6-dien-3-ol, Indole-3-methyl, and Di-isononyl phthalate outperforming the native ligand. Their binding patterns, particularly strong interactions with ASP206, TRP203, and LYS140, reflect significant structural compatibility with the active site of the enzyme. These results support the traditional antidiabetic relevance of Butea monosperma and justify further in vitro and in vivo validation of its lead compounds.

ADMET analysis

The ADMET profiling of the GC-MS-identified constituents of *Butea monosperma* against *α*-amylase (PDB ID: 6Z8L) revealed that several compounds exhibited more favorable druglikeness and toxicity profiles than the native ligand (NL-6Z8L).

From physicochemical analysis (Table 5), NL-6Z8L is a small, highly polar molecule (MW 180.06, Topological Polar Surface Area (TPSA) 110.38, nHA 6, nHD 5) with very high aqueous solubility (logS 0.26) but marked hydrophilicity (logP −2.19). This combination supports good solubility but may limit passive membrane permeability. In contrast, most phytoconstituents, particularly apocynin, benzeneacetic acid, hydrocinnamic acid, *t*-butylhydroquinone, indole-3-methyl, and tyrosol, showed lower TPSA (15.79–66.48) and moderate logP values (approximately 0.1–2.6), which are generally more compatible with the oral drug-like balance between solubility and permeability. Among these, hydrocinnamic acid (MW 150.07, TPSA 37.3, logP 1.90) and benzeneacetic acid (MW 136.05, TPSA 37.3, logP 1.52) displayed favorable sizes and polarities compared with NL-6Z8L, suggesting improved membrane diffusion while retaining sufficient hydrogen bonding capacity. Tyrosol (TPSA 66.48, logP 0.13) and *t*-butylhydroquinone (TPSA 40.46, logP 2.46) also showed an acceptable polarity–lipophilicity compromise relative to the highly hydrophilic NL-6Z8L. Conversely, the high-MW, highly lipophilic phthalate esters [bis(2-ethylhexyl) phthalate, di-isononyl phthalate] and cholesta-4,6-dien-3-ol exhibited extreme logP values (>6.9) and very poor solubility (logS < −6), making them substantially less favorable than NL-6Z8L, despite their strong hydrophobic character. L-prolyl-L-valine (MW 214.13, TPSA 78.43, and logP −0.82) remains more polar than the other phytochemicals, but is still less hydrophilic than NL-6Z8L, potentially improving permeability while maintaining good solubility.

Table 5. Physicochemical properties of selected derivatives

Compounds	MW	Volume	Dense	nHA	nHD	nRot	nRing	TPSA	logS	logP
NL-6Z8L	180.06	156.5173	1.150416	6	5	1	1	110.38	0.257491	-2.19131
Apocynin	136.05	145.4025	0.935679	2	1	1	1	37.3	-1.10565	1.461503
Benzenea cetic acid	136.05	145.4025	0.935679	2	1	2	1	37.3	-1.17206	1.518644
Benzoic acid, 4-ethoxy-, ethyl ester	194.09	206.0807	0.941816	3	0	5	1	35.53	-3.74617	3.369667
Bis(2-ethylhexyl) phthalate	390.28	437.0823	0.892921	4	0	16	1	52.6	-6.14914	6.911518
Cholesta-4,6-dien-3-ol	384.34	444.8395	0.863997	1	1	5	4	20.23	-6.48965	6.983746
Di-isononyl phthalate	418.31	471.6742	0.886862	4	0	18	1	52.6	-7.02634	7.708097
Hydrocin namic acid	150.07	162.6985	0.922381	2	1	3	1	37.3	-1.46267	1.89683
Indole, 3-methyl-	131.07	147.5583	0.888259	1	1	0	2	15.79	-2.33281	2.613684
L-prolyl-L-valine	214.13	216.0511	0.991108	5	3	5	1	78.43	-0.91297	-0.81799

***t*-Butylhydroquinone**	166.1	182.6309	0.909485	2	2	1	1	40.46	-2.19991	2.458687
Tyrosol	167.09	176.3317	0.947589	3	4	3	1	66.48	-1.35965	0.127972

Druglikeness indices (Table 6) further support the superiority of several phenolic acids and small polar molecules over native ligands. NL-6Z8L displays a modest Quantitative Estimate of Druglikeness (QED) of 0.29, whereas hydrocinnamic acid (0.712), benzoic acid derivatives (0.665–0.69), tyrosol (0.604), *t*-butylhydroquinone (0.581), L-prolyl-L-valine (0.614) and apocynin (0.595) all score substantially higher, indicating more favorable combinations of size, polarity, and structural features for drug development. Notably, these high-QED compounds still comply with Lipinski, Pfizer, and GSK rules, similar to NL-6Z8L (Lipinski violations = 0 for all compounds), while also residing within the Golden Triangle space in most cases, suggesting a balanced potency–pharmacokinetics profile. In contrast, the large phthalates and cholesta-4,6-dien-3-ol showed lower QED values (0.21–0.533) and failed the Pfizer and GSK criteria due to excessive lipophilicity and size, making them less attractive than NL-6Z8L despite favorable docking. Overall, the QED analysis indicated that small phenolic acids (hydrocinnamic acid and benzeneacetic acid), phenolic antioxidants (*t*-butylhydroquinone and tyrosol), apocynin, indole-3-methyl, and the dipeptide L-prolyl-L-valine possess superior intrinsic drug-like features compared to the native ligand.

The absorption parameters (Table 7) clearly show that NL-6Z8L demonstrated the highest predicted human intestinal absorption (HIA 0.9756), clearly outperforming all the phytoconstituents, which generally show low HIA values. *t*-Butylhydroquinone (HIA 0.2251) and L-prolyl-L-valine (0.0937) were the best derivatives; however, they did not approach the predicted absorption of NL-6Z8L. However, several compounds exhibited less negative Caco-2 and MDCK permeability values than NL-6Z8L, indicating a potentially improved passive permeability. For example, hydrocinnamic acid (Caco-2 −4.2951, MDCK −4.6164), apocynin (−4.5389, −4.5445), benzeneacetic acid (−4.8238, −4.2662), and indole-3-methyl (−4.4633, −4.6227) can cross biological membranes more readily than the highly hydrophilic NL-6Z8L (−6.4684, −4.9164).

The discrepancy between permeability and HIA predictions may reflect active transport and efflux contributions: NL-6Z8L is strongly predicted as a P-gp substrate (0.7108) without significant inhibitory effects, whereas several phytochemicals show varying degrees of P-gp inhibition (e.g., *t*-butylhydroquinone, benzoic acid 4-ethoxy ethyl ester, and bis(2-ethylhexyl) phthalate), which could modulate their net absorption and potential drug–drug interactions. Overall, NL-6Z8L clearly retained superior predicted oral absorption, but compounds such as hydrocinnamic acid, apocynin, indole-3-methyl, and *t*-butylhydroquinone may exhibit more balanced permeability–lipophilicity properties that can be further optimized.

Table 6. Druglikeness properties of designed derivatives

Compounds	QED	NP score	Lipinski rule	Pfizer rule	GSK rule	Golden triangle	Chelator rule
NL-6Z8L	0.29	2.627	0	0	0	1	0
Apocynin	0.595	0.141	0	0	0	1	0
Benzeneacetic acid	0.665	-0.164	0	0	0	1	0
Benzoic acid, 4-ethoxy-, ethyl ester	0.69	-0.808	0	1	0	1	0
Bis(2-ethylhexyl) phthalate	0.343	0.091	0	1	1	0	0
Cholesta-4,6-dien-3-ol	0.533	2.7	0	1	1	0	0
Di-isononyl phthalate	0.21	0.025	0	1	1	0	0
Hydrocinnamic acid	0.712	0.139	0	0	0	1	0
Indole, 3-methyl-	0.565	-0.326	0	0	0	1	0
L-prolyl-L-valine	0.614	0.087	0	0	0	0	0
***t*-Butylhydroquinone**	0.581	0.757	0	0	0	1	0
Tyrosol	0.604	0.886	0	0	0	1	0

Table 7. Absorption parameter of selected compounds

Compounds	Caco-2 permeability	MDCK permeability	Pgp-inhibitor	Pgp-substrate	HIA	F20%	F30%	F50%
NL-6Z8L	-6.4684	-4.9164	0.000256	0.71083	0.975598	0.60693	0.95796	0.90705
Apocynin	-4.5389	-4.5445	0.090341	0.23952	0.056761	0.22711	0.22685	0.60576
Benzeneacetic acid	-4.8238	-4.2662	1.76E-05	0.00708	0.000204	0.00117	0.00039	0.00729
Benzoic acid, 4-ethoxy-, ethyl ester	-4.7529	-4.6852	0.312205	0.0343	0.066283	0.66275	0.68545	0.82175
Bis(2-ethylhexyl) phthalate	-4.9184	-4.7105	0.499525	0.02053	0.011661	0.62897	0.77261	0.84708
Cholesta-4,6-dien-3-ol	-5.3379	-5.1111	0.000477	0.01441	7.65E-05	0.01285	0.79007	0.99084
Di-isononyl phthalate	-5.1486	-4.7076	0.012012	0.00037	8.95E-05	0.00847	0.2834	0.25543
Hydrocinnamic acid	-4.2951	-4.6164	0.18274	0.01658	0.005374	0.0112	0.05324	0.24221
Indole, 3-methyl-	-4.4633	-4.6227	0.371859	0.20603	0.003074	0.0533	0.16212	0.55416
L-prolyl-L-valine	-6.1861	-5.1226	0.099414	0.05797	0.093692	0.2095	0.812	0.66327
***t*-Butylhydroquinone**	-4.8601	-4.8105	0.317387	0.15544	0.225058	0.90818	0.94723	0.99004
Tyrosol	-5.9409	-4.9452	0.000102	0.96418	6.72E-05	0.02541	0.00686	0.58964

The distribution and metabolism profile (Table 8) revealed important differences between NL-6Z8L and its phytoconstituents. NL-6Z8L displayed relatively low plasma protein binding (PPB 29.28 %) and a negative volume of distribution (VD −0.4685), indicating limited tissue penetration, but a high free fraction (Fu 74.52 %), which may contribute to the rapid onset at the target site. In contrast, most small aromatic acids and phenolics, such as apocynin, benzeneacetic acid, and hydrocinnamic acid, show high PPB values (84–96 %) and moderate VD,

implying a more restricted free circulating drug but potentially prolonged systemic exposure compared with NL-6Z8L. L-prolyl-L-valine and tyrosol, similar to the native ligand, retained lower PPB (19.37 and 31.05 %, respectively) and higher free fractions (>70 %), making their free drug profile closer to that of NL-6Z8L. Regarding BBB penetration, NL-6Z8L had a moderate BBB index (0.4811), whereas the highly lipophilic indole-3-methyl (0.9225) and cholesta-4,6-dien-3-ol (0.6679) were more likely to cross the blood–brain barrier, which may not be desirable for a peripherally acting α-amylase inhibitor. CYP interaction patterns further distinguish these molecules: NL-6Z8L shows very low predicted inhibition and substrate probabilities across CYP isoforms, suggesting minimal metabolic drug–drug interaction risk. In contrast, several phytochemicals, especially benzoic acid 4-ethoxy ethyl ester, bis(2-ethylhexyl) phthalate, di-isononyl phthalate, indole-3-methyl, and cholesta-4,6-dien-3-ol, display high probabilities of CYP1A2, CYP2C19, CYP2C9, CYP2D6, and CYP3A4 inhibition and/or substrate behavior.

Table 8. Distribution and metabolism parameter of selected molecules

Compounds	Distribution				Metabolism									
					CYP1A2		CYP2C19		CYP2C9		CYP2D6		CYP3A4	
	PPB%	VD	BBB	Fu	Inhibitor	Substrate	Inhibitor	Substrate	Inhibitor	Substrate	Inhibitor	Substrate	Inhibitor	Substrate
NL-6Z8L	29.2818	-0.4685	0.48106	74.5164	0.008555	0.000523	1.79E-05	6.15E-05	0.00432	0.351505	0.017161	1.27E-05	0.000132	2.62E-05
Apocynin	84.7721	0.00888	0.20025	17.1447	0.801273	0.082775	0.208392	0.066812	0.086652	0.004572	0.047664	0.164116	0.088635	0.001676
Benzeneacetic acid	84.4163	-0.6133	0.27844	12.8771	0.007617	0.00598	0.008822	0.001841	0.042731	0.365265	0.000225	0.001785	1.35E-05	0.059231
Benzoic acid, 4-ethoxy-, ethyl ester	92.3756	0.36599	0.02866	8.84443	0.998367	0.991312	0.996111	0.95132	0.925221	0.845996	0.480613	0.457466	0.103553	0.002692
Bis(2-ethylhexyl) phthalate	98.6603	0.93984	0.98948	1.3982	0.562833	0.00114	0.999076	0.610825	0.651027	0.001848	0.050312	1.28E-06	0.966199	0.987692
Cholesta-4,6-dien-3-ol	72.1716	-0.2592	0.66791	23.213	0.000122	0.000188	0.977623	0.988268	0.730986	0.000616	0.09866	0.001718	0.923081	1

Di-isononyl phthalate	98.1452	0.88684	0.43794	2.66951	0.284994	5.39E-06	1	0.004598	0.996975	2.27E-05	0.747633	1.05E-08	0.979165	0.999998
Hydrocinnamic acid	96.4636	-0.4405	0.09531	3.20483	0.001258	0.000787	0.003265	0.001064	0.014737	0.998878	0.008055	0.284985	4.70E-07	0.001947
Indole, 3-methyl-	83.7547	0.06969	0.9225	12.217	0.999802	0.790341	0.976467	0.143063	0.10048	0.926136	0.432301	0.984595	0.696616	0.450438
L-prolyl-L-valine	19.3706	-0.3771	0.00552	76.8816	7.50E-09	1.12E-07	1.88E-06	0.012075	2.00E-07	0.407679	4.09E-05	0.009377	1.18E-05	6.86E-05
***t*-Butylhydroquinone**	66.847	0.25533	0.00909	32.5606	0.585854	0.049622	0.135148	0.037531	0.036698	0.491551	0.148221	0.818319	0.006229	0.273666
Tyrosol	31.0517	0.2481	0.00457	70.9975	6.39E-07	1.62E-05	6.84E-07	0.11118	1.35E-10	0.001604	0.003477	1	9.53E-05	0.198522

These interactions may lead to complex metabolism, altered clearance, and increased interaction risk relative to those of native ligands. More favorable in this regard are tyrosol and L-prolyl-L-valine, which, like NL-6Z8L, show a low CYP inhibition likelihood and limited substrate liabilities. Excretion and toxicity endpoints (Table 9) highlight several instances where phytoconstituents improve the safety profile of NL-6Z8L. The native ligand exhibited moderate plasma clearance (CL 2.20) and half-life (T1/2 1.96), and it was flagged with relatively high probabilities of hepatotoxicity (H-HT 0.5608), drug-induced liver injury (DILI 0.6189), and Ames mutagenicity (0.9008). In contrast, many phytochemicals, such as hydrocinnamic acid (H-HT 0.396, DILI 0.1084, Ames 0.1848), *t*-butylhydroquinone (H-HT 0.2862, DILI 0.0979, Ames 0.2486), apocynin (H-HT 0.4156, DILI 0.1877, Ames 0.3935), and benzeneacetic acid (H-HT 0.3695, DILI 0.9113, but low Ames 0.1355), generally show reduced mutagenic liability compared to NL-6Z8L. Tyrosol is noteworthy for simultaneously showing a high hepatotoxicity probability (H-HT 0.9202) but a low DILI prediction (0.0623), indicating that while some hepatic risk cannot be ruled out, overall clinically significant injury may still be limited. Large hydrophobic phthalates exhibit low Ames scores, but their other safety aspects and environmental concerns make them less suitable than smaller phenolics. Several phytoconstituents, including L-prolyl-L-valine and tyrosol, also showed high FDAMDD values and low skin sensitization or carcinogenicity probabilities, suggesting acceptable systemic safety compared with the native ligand. Thus, although NL-6Z8L is favorable in terms of absorption, it appears to carry higher mutagenicity and liver injury risk than many phenolic and small polar constituents.

Table 9. Excretion and toxicity parameters of selected compounds

Compounds	Excretion			Toxicity							
	CL-plasma	T1/2	H-HT	DILI	Ames Toxicity	Rat Oral Acute Toxicity	FDAMDD	Skin Sensitization	Carcinogenicit	Eye Corrosion	Eye Irritation	Respiratory Toxicity
NL-6Z8L	2.20004	1.96452	0.56084	0.61887	0.90075	0.07459	0.01237	0.993052	0.23581	0.05826	0.95787	0.06779
Apocynin	11.1498	1.09619	0.41557	0.187684	0.39354	0.15683	0.21026	0.689175	0.61023	0.94303	0.99866	0.60389
Benzeneacetic acid	0.90638	1.69803	0.3695	0.911299	0.13554	0.36916	0.02766	0.89729	0.19715	0.98535	0.99787	0.37734
Benzoic acid, 4-ethoxy-, ethyl ester	9.27877	0.5859	0.06954	0.710298	0.27	0.13664	0.11765	0.089303	0.70877	0.17162	0.98618	0.22745
Bis(2-ethylhexyl) phthalate	5.78999	0.32392	0.08584	0.106304	0.01809	0.04349	0.21445	0.937571	0.32825	0.52187	0.97883	0.28255
Cholesta-4,6-dien-3-ol	10.8557	0.35356	0.74222	0.51833	0.38847	0.26702	0.59914	0.858285	0.75269	0.1239	0.89429	0.90117
Di-isononyl phthalate	5.93017	0.27329	0.04007	0.156203	0.02378	0.02457	0.04107	0.726442	0.85389	0.43633	0.9951	0.04778
Hydrocinnamic acid	3.30652	1.46783	0.3958	0.108411	0.18479	0.18589	0.14356	0.453633	0.23444	0.8979	0.99414	0.37709
Indole, 3-methyl-	9.46128	1.47969	0.58746	0.485981	0.63733	0.52722	0.33564	0.546476	0.66648	0.8226	0.99044	0.74475

L-prolyl-L-valine	4.62607	1.46926	0.19038	0.688618	0.48729	0.57444	0.12665	0.995173	0.11834	0.20469	0.97162	0.92847
***t*-Butylhydroquinone**	13.0525	1.26574	0.28619	0.097917	0.24855	0.41321	0.50285	0.775855	0.4059	0.96849	0.99759	0.72877
Tyrosol	12.6671	1.6604	0.92022	0.062268	0.29778	0.65836	0.57895	0.97613	0.04021	0.95379	0.97553	0.84374

Table 10. Environmental toxicity profile of designed molecules

Compounds	BCF	IGC50	LC50FM	LC50DM
NL-6Z8L	0.126745	1.441309	1.891225	2.586628
Apocynin	0.648696	2.728015	2.87166	3.501175
Benzeneacetic acid	0.155867	2.411207	2.765902	3.353576
Benzoic acid, 4-ethoxy-, ethyl ester	1.538367	4.061689	4.453395	4.961454
Bis(2-ethylhexyl) phthalate	1.280301	3.911522	1.306083	4.259209
Cholesta-4,6-dien-3-ol	3.100443	4.765406	5.493543	5.370886
Di-isononyl phthalate	0.591982	3.703802	2.560851	5.630079
Hydrocinnamic acid	0.177709	2.788499	3.163065	3.752216
Indole, 3-methyl-	1.769279	3.35684	4.155183	4.360415
L-prolyl-L-valine	0.08101	2.758135	3.476957	4.200885
***t*-Butylhydroquinone**	1.772945	4.524278	4.954678	5.276406
Tyrosol	0.603198	2.402533	3.082412	3.584935

The environmental toxicity profiles (Table 10) provide an additional differentiating layer between the native ligand and phytoconstituents. NL-6Z8L showed a low bioconcentration factor (BCF 0.127) and moderate aquatic toxicity indices (IGC_{50} 1.44, LC_{50}FM 1.89, and LC_{50}DM 2.59), suggesting limited environmental bioaccumulation but non-negligible toxicity to aquatic species. Several small phenolics and acids, such as L-prolyl-L-valine (BCF 0.0810), hydrocinnamic acid (0.1777), benzeneacetic acid (0.1559), and tyrosol (0.6032), maintained similarly low or only moderately higher BCF values than NL-6Z8L but generally had higher LC50/IGC50 values, indicating lower acute aquatic toxicity. In contrast, lipophilic compounds, such as cholesta-4,6-dien-3-ol (BCF 3.10), *t*-butylhydroquinone, and indole-3-methyl (BCF ~1.77), showed higher bioaccumulation potential, which may pose long-term environmental hazards despite favorable LC50 metrics. On balance, small, moderately lipophilic compounds such as hydrocinnamic acid and L-prolyl-L-valine align more closely with or even improve the environmental profile of NL-6Z8L, while highly lipophilic phthalates and sterols are less attractive from an ecotoxicological perspective.

Table 11. ADMET radar of all selected compounds

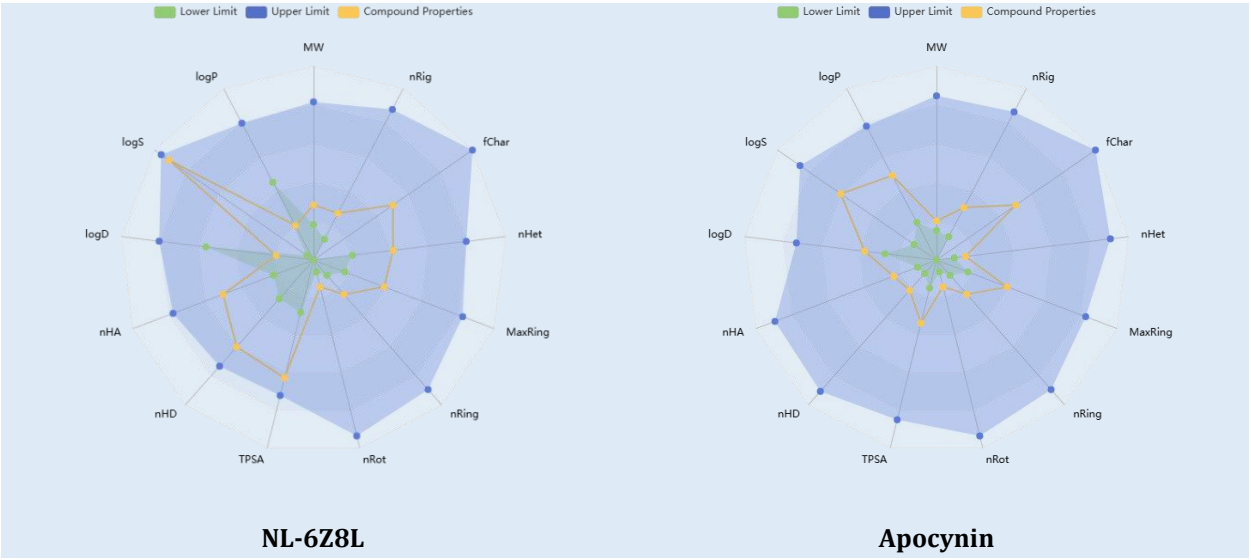

NL-6Z8L

Apocynin

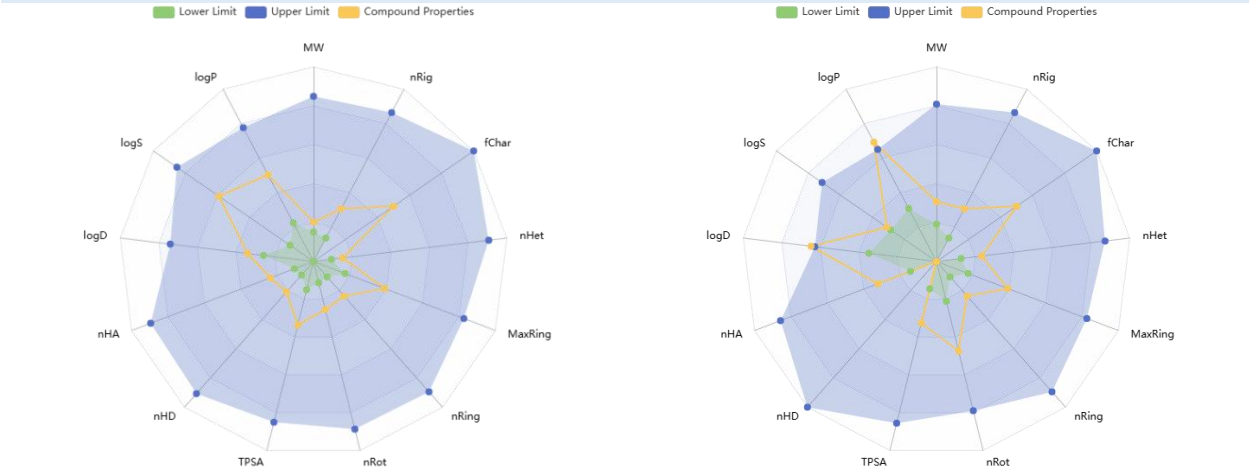

Benzeneacetic acid

Benzoic acid, 4-ethoxy-, ethyl ester

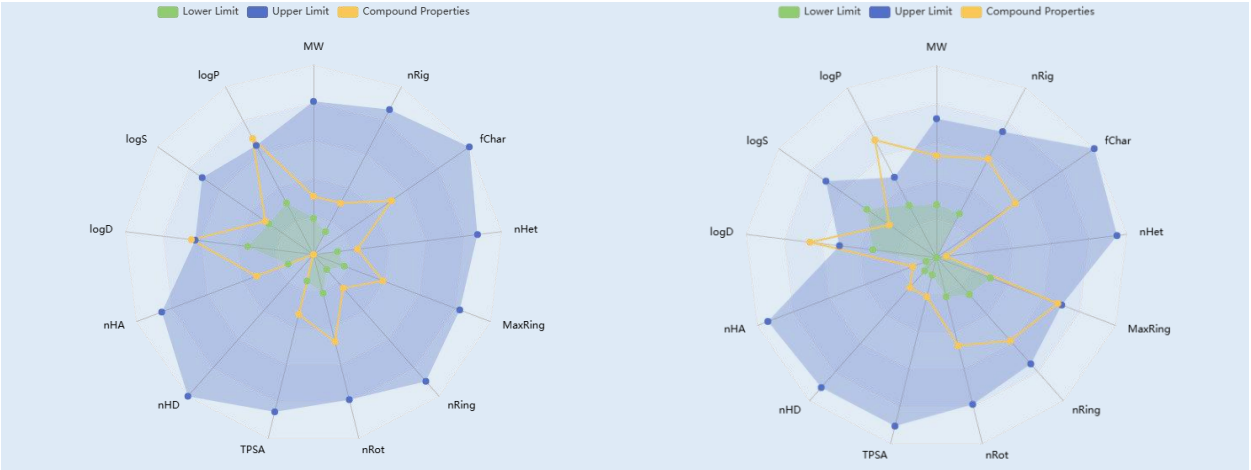

Bis(2-ethylhexyl) phthalate

Cholesta-4,6-dien-3-ol

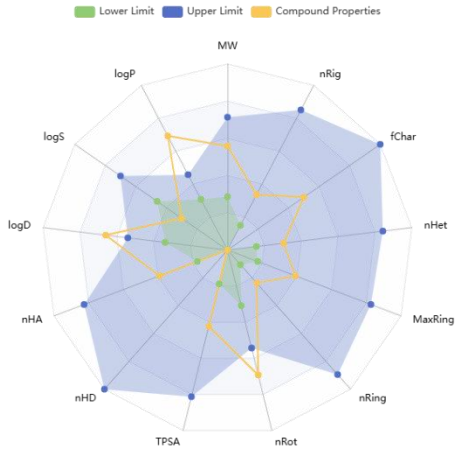

Di-isononyl phthalate

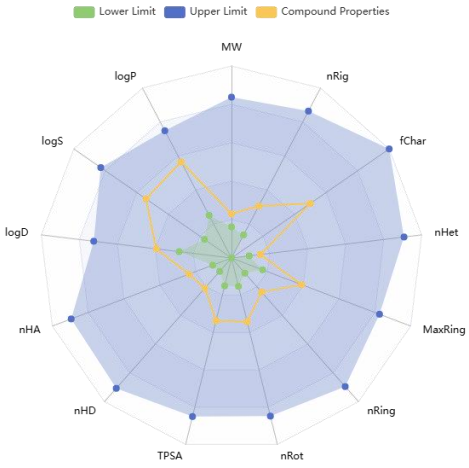

Hydrocinnamic acid

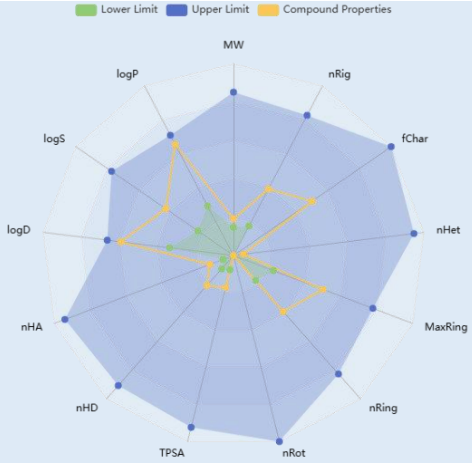

Indole, 3-methyl-

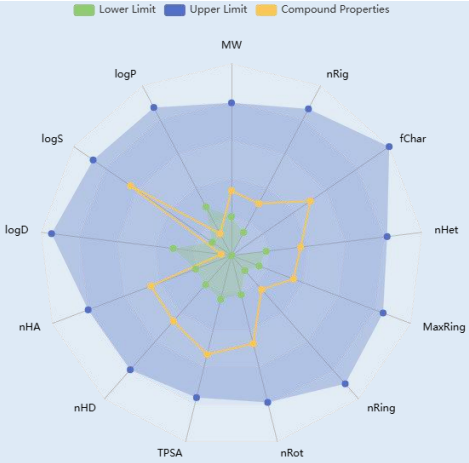

L-prolyl-L-valine

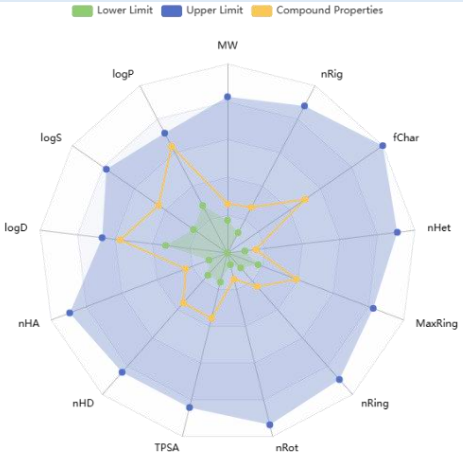

***t*-Butylhydroquinone**

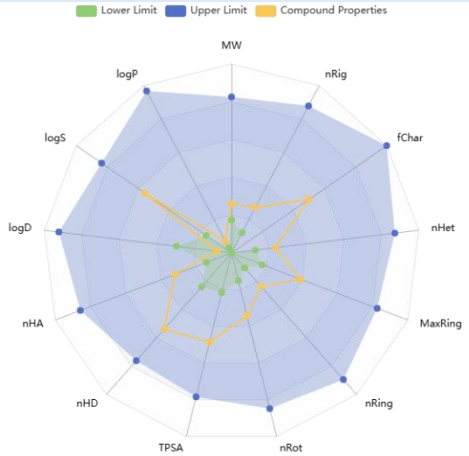

Tyrosol

Integrating all parameters, NL-6Z8L serves as a highly soluble, well-absorbed reference ligand with limited distribution and low CYP liabilities but a somewhat unfavorable safety signature, particularly for Ames mutagenicity and DILI risk. In comparison, several *Butea monosperma* phytoconstituents, especially hydrocinnamic acid, benzeneacetic acid, apocynin, indole-3-methyl, *t*-butylhydroquinone, tyrosol, and L-prolyl-L-valine, display superior druglikeness (higher QED), more balanced lipophilicity, acceptable or improved metabolic and toxicity profiles, and comparable or reduced environmental impacts. Although most of these compounds showed lower predicted HIA than NL-6Z8L, their more favorable physicochemical and safety characteristics suggest that upon appropriate structural optimization or formulation strategies, they could be developed into safer and more drug-like *α*-amylase inhibitors than the native ligand. Among them, hydrocinnamic acid, *t*-butylhydroquinone, and L-prolyl-L-valine stand out for combining good drug-likeness, manageable distribution and metabolism, reduced mutagenicity, and acceptable environmental behavior, making them promising lead candidates in comparison with the NL-6Z8L ADMET radar for all selected compounds with native ligands, as shown in Table 11.

Conclusion

Comprehensive phytochemical, GC–MS, molecular docking, and ADMET analyses collectively highlight *Butea monosperma* as a promising natural source of *α*-amylase inhibitory compounds. The hydroalcoholic extract exhibited excellent physicochemical stability, microbial safety, and abundance of bioactive secondary metabolites, particularly phenolics, flavonoids, tannins, glycosides, and cyclic dipeptides. GC–MS profiling further confirmed a diverse chemical composition dominated by antioxidant and anti-inflammatory constituents such as hydrocinnamic acid, tyrosol, apocynin, and diketopiperazines. Docking studies revealed that several identified compounds, most notably cholesta-4,6-dien-3-ol, indole-3-methyl, and di-isononyl phthalate, demonstrated stronger binding affinities toward *α*-amylase than the native ligand (NL-6Z8L), forming stable interactions with key catalytic residues, such as ASP206, TRP203, and LYS140. ADMET evaluation supported the drug-like nature and favorable safety profiles of smaller phenolic molecules, including hydrocinnamic acid, apocynin, *t*-butylhydroquinone, tyrosol, and L-prolyl-L-valine, many of which exhibited lower predicted toxicity and improved pharmacokinetic balance than the native ligand. Overall, these findings validate the therapeutic potential of *Butea monosperma* as a source of natural *α*-amylase inhibitors and support its traditional antidiabetic applications. Future studies should focus on targeted *in vitro* and *in vivo* investigations, followed by formulation development, to translate these promising leads into effective antidiabetic interventions.

Disclosure Statement

No potential conflict of interest was reported by the authors.

ORCID

Rupasrre Peruru:
https://orcid.org/0000-0001-8665-8273
Manasa Sathoori:
https://orcid.org/0009-0006-3201-5436
Venkata Ramana Singamaneni:
https://orcid.org/0009-0006-4328-8253
Pradeep Vidiyala:
https://orcid.org/0009-0003-3130-9879
Ramenani Hari Babu:
https://orcid.org/0009-0006-6396-2110
Om M. Bagade:
https://orcid.org/0000-0002-5398-2752
Reehana Shaik:
https://orcid.org/0000-0002-8413-713X
CH. K. V. L. S. N Anjana Male:
https://orcid.org/0000-0001-9032-8314

References

[1] Khan, A., Unnisa, A., Sohel, M., Date, M., Panpaliya, N., Saboo, S.G., Siddiqui, F., Khan, S. Investigation of phytoconstituents of enicostemma littorale as potential glucokinase activators through molecular docking for the treatment of type 2 diabetes mellitus. *In Silico Pharmacology*, **2021**, 10(1), 1.

[2] Shastri, M.A., Gadhave, R., Talath, S., Wali, A.F., Hani, U., Puri, S., Rathod, B., Khan, S.L. In silico screening, synthesis, and in vitro enzyme assay of some 1, 2, 3-oxadiazole-linked tetrahydropyrimidine-5-carboxylate derivatives as DPP-IV inhibitors for treatment of T2DM. *Chemical Methodologies*, **2024**, 8(11), 800-819.

[3] Suryawanshi, R.M., Shimpi, R.B., Muralidharan, V., Nemade, L.S., Gurugubelli, S., Baig, S., Vikhe, S.R., Dhawale, S.A., Mortuza, M.R., Sweilam, S.H. Adme, toxicity, molecular docking, molecular dynamics, glucokinase activation, DPP-IV, α-amylase, and α-glucosidase inhibition assays of mangiferin and friedelin for antidiabetic potential. *Chemistry & Biodiversity*, **2025**, 22(5), e202402738.

[4] Jadhav, P.B., Jadhav, S.B., Zehravi, M., Mubarak, M.S., Islam, F., Jeandet, P., Khan, S.L., Hossain, N., Rashid, S., Ming, L.C. Virtual screening, synthesis, and biological evaluation of some carbohydrazide derivatives as potential DPP-IV inhibitors. *Molecules*, **2022**, 28(1), 149.

[5] Kashtoh, H., Baek, K.H. New insights into the latest advancement in α-amylase inhibitors of plant origin with anti-diabetic effects. *Plants*, **2023**, 12(16), 2944.

[6] Kumar, B.A., Lakshman, K., Nandeesh, R., Kumar, P.A., Manoj, B., Kumar, V., Shekar, D.S. In vitro alpha-amylase inhibition and in vivo antioxidant potential of amaranthus spinosus in alloxan-induced oxidative stress in diabetic rats. *Saudi Journal of Biological Sciences*, **2011**, 18(1), 1-5.

[7] Tandon, R., Shivanna, K., Mohan Ram, H. Reproductive biology of butea monosperma (fabaceae). *Annals of Botany*, **2003**, 92(5), 715-723.

[8] Rai, A., Pandey, V.C., Singh, A.K., Ghoshal, N., Singh, N. Butea monosperma: A leguminous species for sustainable forestry programmes. *Environment, Development and Sustainability*, **2021**, 23(6), 8492-8505.

[9] Sindhia, V., Bairwa, R. Plant review: Butea monosperma. *International Journal of Pharmaceutical and Clinical Research*, **2010**, 2(2), 90-94.

[10] Pattanayak, S., Mollick, M.M.R., Maity, D., Chakraborty, S., Dash, S.K., Chattopadhyay, S., Roy, S., Chattopadhyay, D., Chakraborty, M. Butea monosperma bark extract mediated green synthesis of silver nanoparticles: Characterization and biomedical applications. *Journal of Saudi Chemical Society*, **2017**, 21(6), 673-684.

[11] Seetharaman, J., Priya, R.A., Philip, R.R., Muthuraj, M., Sankari, D. Evaluation of tridax procumbens secondary metabolites anti-tuberculosis activity by in vitro and in silico methods. *Current Microbiology*, **2025**, 82(1), 50.

[12] Maulydia, N., Idroes, R., Khairan, K., Tallei, T., Mohd Fauzi, F. Ecotoxicological insight of phytochemicals, toxicological informatics, and heavy metal concentration in tridax procumbens l. In geothermal areas. *Geothermal Areas, Global Journal of Environmental Science and Management*, **2024**, 10(1), 369-384.

[13] Ukwubile, C., Mathias, S., Pisagih, P. Acute and subchronic toxicity evaluation and gc-ms profiling of ajumbaise: A traditional nigerian polyherbal formulation for labor enhancement and pain relief. *Journal of Pharmaceutical Sciences and Computational Chemistry*, **2025**, 1(2), 154-173.

[14] Tamboli, A., Tayade, S. In-depth investigation of berberine and tropane through computational screening as possible DPP-IV inhibitors for the treatment of t2dm. *Journal of Pharmaceutical Sciences and Computational Chemistry*, **2025**, 1(1), 1-11.

[15] Siddiqui, F., Makhloufi, R., Salah, M.E.-S., Mohamed, E., Hojjati, M. Computational exploration of quinine and mefloquine as potential anti-malarial agents. *Journal of Pharmaceutical Sciences and Computational Chemistry*, **2025**, 1(2), 106-115.

[16] Ahmed, S., Tabassum, P., Falak, S., Ahmad, A., Shaikh, M. Molecular docking and network pharmacology: Investigating vitis vinifera phytoconstituents as multi-target therapeutic agents against breast cancer. *Journal of Pharmaceutical Sciences and Computational Chemistry,* **2025**, 1(2), 116-134.

[17] Jadhav, S., Dighe, P. In vitro evaluation, and molecular docking studies of novel pyrazoline derivatives as promising bioactive molecules. *Journal of Pharmaceutical Sciences and Computational Chemistry,* **2025**, 1(3), 190-209.

[18] Benitez, R.B., Bonilla, R.A.O., Franco, J.M. Comparison of two sesame oil extraction methods: Percolation and pressed. *Biotecnología en el Sector Agropecuario y Agroindustrial*, **2016**, 14(1), 10-18.

[19] Ravanfar, R., Moein, M., Niakousari, M., Tamaddon, A. Extraction and fractionation of anthocyanins from red cabbage: Ultrasonic-assisted extraction and conventional percolation method. *Journal of Food Measurement and Characterization*, **2018**, 12(4), 2271-2277.

[20] Khandelwal, K.R. Practical Pharmacognosy. *Book*, **2005**, 150-153.

[21] Mukherjee, P.K. Quality control of herbal drugs: An approach to evaluation of botanicals. Business Horizons: New Delhi, India, **2002**, 10–800.
[22] Singh, M., Tamboli, E., Kamal, Y., Ahmad, W., Ansari, S., Ahmad, S. Quality control and in vitro antioxidant potential of coriandrum sativum linn. *Journal of Pharmacy and Bioallied Sciences*, **2015**, 7(4), 280-283.
[23] Kamal, Y., Singh, M., Salam, S., Ahamd, S. Standardization of unani polyherbal formulation, qurse-e-hummaz: A comprehensive approach. *Drug Development and Therapeutics*, **2016**, 7(1), 39-39.
[24] Chaudhari, R.N., Khan, S.L., Chaudhary, R.S., Jain, S.P., Siddiqui, F. B-sitosterol: Isolation from muntingia calabura linn bark extract, structural elucidation and molecular docking studies as potential inhibitor of sars-cov-2 mpro (covid-19). *Asian Journal of Pharmaceutical and Clinical Research*, **2020**, 13, 204-209.
[25] Indrayanto, G. Recent development of quality control methods for herbal derived drug preparations. *Natural Product Communications*, **2018**, 13(12), 1934578X1801301208.
[26] Al-Busaid, M., Akhtar, M., Alam, T., Shehata, W. Development and evaluation of herbal cream containing curcumin from curcuma longa. *Pharmacy and Pharmacology International Journal*, **2020**, 8(5), 285-289.
[27] Xu, Y., Ou, Q., Wang, X., Hou, F., Li, P., van der Hoek, J.P., Liu, G. Assessing the mass concentration of microplastics and nanoplastics in wastewater treatment plants by pyrolysis gas chromatography–mass spectrometry. *Environmental Science & Technology*, **2023**, 57(8), 3114-3123.
[28] Lisec, J., Schauer, N., Kopka, J., Willmitzer, L., Fernie, A.R. Gas chromatography mass spectrometry–based metabolite profiling in plants. *Nature Protocols*, **2006**, 1(1), 387-396.
[29] Gould, O., Nguyen, N., Honeychurch, K.C. New applications of gas chromatography and gas chromatography-mass spectrometry for novel sample matrices in the forensic sciences: A literature review. *Chemosensors*, **2023**, 11(10), 527.
[30] Valdez, C.A. Gas chromatography-mass spectrometry analysis of synthetic opioids belonging to the fentanyl class: A review. *Critical Reviews in Analytical Chemistry*, **2022**, 52(8), 1938-1968.
[31] Khan, S.L., Bakshi, V. LC-HRMS and in silico analysis of Ailanthus excelsa metabolites targeting egfr triple mutation (L858R/T790M/C797S). *Advanced Journal of Chemistry, Section A*, **2026**, 9(2), 292-311.
[32] Fu, L., Shi, S., Yi, J., Wang, N., He, Y., Wu, Z., Peng, J., Deng, Y., Wang, W., Wu, C. Admetlab 3.0: An updated comprehensive online admet prediction platform enhanced with broader coverage, improved performance, api functionality and decision support. *Nucleic Acids Research*, **2024**, 52(W1), W422-W431.

HOW TO CITE THIS ARTICLE

R. Peruru, M. Sathoori, V.R. Singamaneni, P. Vidiyala, R.H. Babu, O.M. Bagade, R. Shaik, C.K.V.L.S.N A. Male. GC-MS Phytochemical Profiling and Computational Analysis of *Butea monosperma* Plant for Antidiabetic α-Amylase Inhibition. *Adv. J. Chem. A*, 2026, 9(7), 1309-1335.

DOI: 10.48309/AJCA.2026.571603.2024
URL: https://www.ajchem-a.com/article_240976.html